Vibrational states and optical transitions in hydrogen bonds

1998 J. Phys.: Condens. Matter 10 2241

(http://iopscience.iop.org/0953-8984/10/10/008)

J. Phys.: Condens. Matter **10** (1998) 2241–2260. Printed in the UK PII: S0953-8984(98)84787-5

Vibrational states and optical transitions in hydrogen bonds

P G Johannsen

Fachbereich Physik, Universität GH Paderborn, D-33095 Paderborn, Germany

Received 30 May 1997, in final form 28 November 1997

Abstract. Proton energies in hydrogen bonds are mostly calculated using a double Morse potential (the DMP model). This form, however, does not reproduce the experimentally observed correlation between the proton stretching frequency and the bond length in an extended bond-length region sufficiently well. An alternative potential is proposed in the present paper. The quantum states of this non-symmetric double-well potential are calculated numerically using the Numerov (Fox–Goodwin) algorithm. It is shown that the optical spectra of hydrogen bonds in various substances can be well approximated on the basis of the transition frequencies and intensities predicted by the present model. For weakly interacting OH impurities in $LiNbO_3$, the overtone spectrum and line intensities are well reproduced, whereas the line broadenings and the decrease of the fundamental stretching frequencies in intermediate and strong hydrogen bonds are traced back to the influence of the reduced height of the central barrier. The model is also extrapolated to the range of symmetric hydrogen bonds, and the calculated transition frequencies are discussed with respect to most recent infra-red experiments on ice under strong compression. A possible artificial infra-red signal from strained diamond anvils is thereby noted.

1. Introduction

In the DMP model for the description of O–H $\cdots$ O hydrogen bonds, two identical Morse functions $u_M(r)$ are placed back to back to form a symmetric double-well potential $U_{DMP}(r) = u_M(r) + u_M(-r - R)$ [1–10], where R stands for the space between the two neighbouring oxygen atoms, i.e. the bond length. Depending on the chemical environment, bond lengths exhibit values in a range $R \approx$ 242–300 pm [11], and a strong correlation between R and the proton stretching frequency $\nu(R)$ has been observed [11]. For a specific substance, R can be changed by the application of external pressure [2, 8–10], and the $\nu(R)$ dependence was used as a 'fingerprint' for the existence of H bonds [12].

It was noted that the OH distance r_{OH} is also correlated to the bond length R [11, 13], and that this correlation can be described in the DMP model using a common set of parameters [2, 7]. This presupposition of a universal DMP was often adopted to describe the properties of hydrogen bonds in various materials [9, 10], and to predict the behaviour of H bonds with the variation of R, e.g., in H_2O ice under hydrostatic pressure [8], using the parameters of reference [2]. In this particular case, a high-pressure phase ('ice X') was predicted, where the protons occupy the mid-point between the two oxygen atoms, forming a symmetric H bond [2, 8, 14]. The assumption of a universal DMP has also conversely been used to argue that OH impurities do not form hydrogen bonds in $LiNbO_3$, because the experimentally observed overtone spectrum is at variance with the DMP model, and thus a single-oscillator model has been proposed for this system [15].

0953-8984/98/102241+20$19.50

On the other hand, the concept of a universal DMP appears to be questionable. From a neutron diffraction study on highly compressed ice, it was concluded [16] that the variation of the OH distance with R is much smaller than predicted by the DMP model of reference [2], and DMPs have been used in connection with rather different sets of parameters to model the properties of H bonds in different materials [3–6]. Furthermore, IR measurements on the proton stretching frequency in OH:$LiNbO_3$ under pressure showed a frequency shift with a negative mode-Grüneisen parameter [17], following the $\nu(R)$ correlation of weak H bonds [11, 18–22], which can only be described by means of a single-oscillator model [15] at the expense of R-dependent model parameters.

For H_2O ice the proton stretching frequency is expected to exhibit a minimum at the transition to the proposed phase ice X [8, 23, 24], indicating the symmetrization of the H bonds. However, various spectroscopic investigations on highly compressed ice gave no clear evidence for this symmetrization. In Raman measurements, the frequency of the proton stretching modes firstly decreased according to the $\nu(R)$ correlation, but in the range in which the transition to ice X was expected, the lines were no longer detectable [25]. The disappearance of the lines was explained on the assumption that in the proposed crystal structure of ice X, the proton stretching modes are not Raman active. However, in complementary IR spectroscopic investigations up to 110 GPa, the IR absorption lines also disappeared in the pressure range in question [24, 26]. Because of this somewhat controversial situation, the problem of proton potentials in hydrogen bonds is reinvestigated in the present paper.

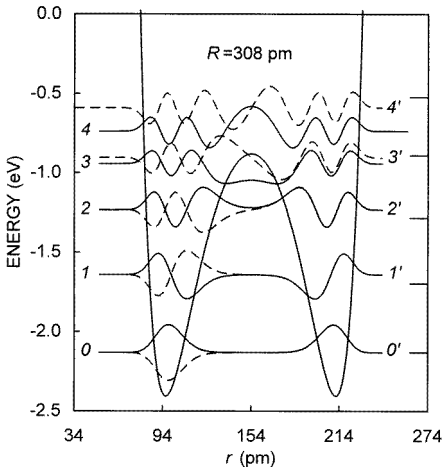

Figure 1. The symmetric double Morse potential with the parameters of reference [15], and the proton wave functions, calculated with the Numerov algorithm (see the appendix). The baselines of the wave functions have been shifted to represent the energy levels. The short lines on the right-hand frame represent the energy levels in OH:$LiNbO_3$, according to the measurements of reference [15]. The states are described by symmetric and anti-symmetric wave functions and are doubly degenerate below the barrier top.

In section 2, the theoretical approach will be outlined, with a special emphasis on the differences between symmetric and non-symmetric potentials. This discussion is of particular importance, because the existence of double-well potentials is often questioned by arguments concerning the localization of protons. It will be shown that non-symmetric double-well potentials are not in contradiction to localized proton states, and that the

phenomenon of coherent tunnelling and delocalized proton states must be seen in connection with the exceptional case of a symmetric potential.

Section 3 will present examples of the present model for different bond lengths, and these results will be discussed in relation to corresponding experimental results on various substances. It will be demonstrated that the present model reproduces the observed frequency–bond-length correlation, and, furthermore, the observed line broadenings in intermediate and strong hydrogen bonds will be related to lifetime broadenings of the ground and first excited states, caused by incoherent tunnelling.

At present, there is considerable activity whose objective is observing the proton stretching frequency of symmetric bonds in ice. Several IR experiments have been performed on this substance at pressures around 100 GPa and above. However, the results of these experiments do not seem to give clear evidence for the expected proton mode in symmetric bonds. The predictions of the present model for the transitions in symmetric bonds will be discussed in connection with these most recent results.

In an appendix, the more technical details of the present calculations will be given and the mathematical advantages of the proposed potential, making it also suitable for other applications, will be discussed.

2. Theory

The time-independent one-dimensional Schrödinger equation

$$\left[-\frac{\hbar^2}{2\mu}\,\frac{\mathrm{d}^2}{\mathrm{d}r^2}+U(r)\right]\Psi(r)=E\Psi(r) \tag{1}$$

can only be solved analytically in some rare cases, e.g., for the single Morse potential. Thus, the wave functions and eigenstates are often calculated using the semi-classical WKB method [3–6], or a variational approach [8–10]. The WKB approximation, however, is accompanied by conceptual and computational problems, and, because of its semi-classical character, it is not clear in special cases to what extent the results are reliable. Variational approaches, on the other hand, are generally useful for the calculation of the ground-state wave functions only. In this work, equation (1) has been solved numerically (see the appendix).

A hydrogen bond in a solid may be symbolized by X_1–O–H$\cdots$O–X_2, where X_1 and X_2 stand for the interactions with the rest of the crystal, 'seen' by the left-hand and right-hand oxygens, respectively. If $X_1 = X_2$, the proton potential must be a symmetric double-minimum potential, irrespective of the oxygen–oxygen distance, because the positions near the oxygens cannot be distinguished. In the case $X_1 \neq X_2$, the proton potential is non-symmetric.

In the traditional DMP model, the proton potential in weak hydrogen bonds originates primarily from the OH bond, described by a Morse function. The influence of the second oxygen is taken into account by the same function, resulting in a double-minimum potential. In most previous treatments using the DMP model, symmetric DMPs were considered, thus implicitly assuming the case $X_1 = X_2$. Figure 1 represents the wave functions and energy levels in such a symmetric DMP. The energy levels far below the barrier top are doubly degenerate with totally symmetric and anti-symmetric wave functions relative to the bond centre. The proton states are therefore delocalized with equal probability in both wells, which corresponds to coherent tunnelling of the protons. Near the barrier top, the degeneracy is destroyed by tunnel splitting.

Coherent tunnelling is an interesting quantum effect, and there is at present considerable activity in searching for examples of tunnel splitting in solids. However, as a rule, proton states in solids are localized, and, up to now, there seems to have been only one exception from this rule, where coherent tunnelling has been identified in a solid [27]. There are different reasons for the localization of protons [28]. On the one hand, static interactions with $X_1 \neq X_2$ are generally accompanied by an energy bias in the proton potential, which, as discussed below, leads to proton localization. On the other hand, due to X_1 and X_2, the two oxygen atoms can also be coupled to lattice vibrations, by which the proton potential is modulated. These dynamic distortions of the potential are generally not in phase with a possible coherent tunnelling motion, and coherence is destroyed even in the case $X_1 = X_2$, when the hydrogen bond is coupled to a phonon bath, and the proton states localize. Thus, the traditional DMP model applies only to an exceptional case, whereas for a more general description of hydrogen bonds, non-symmetric potentials have to be considered.

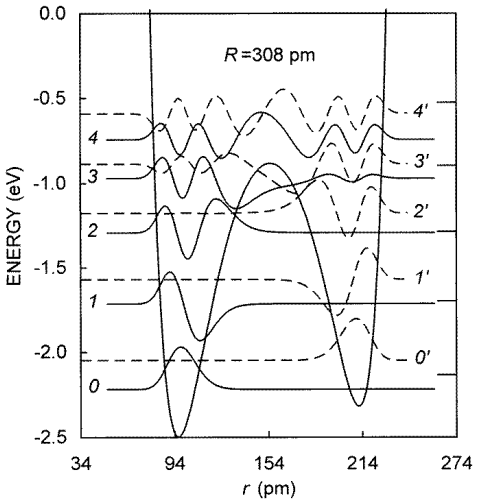

Figure 2. Proton states in a non-symmetric DMP $U_{DMP}(r) = cu_M(r) + c^{-1}u_M(-r - R)$, with $c = 1.04$ and the same potential parameters as in figure 1. The states below the barrier top are localized and the degeneracy is lifted due to the energy bias.

Figure 2 represents a non-symmetric DMP and its quantum states. The deep-level states are considerably different from the corresponding states in the symmetric potential: the degeneracy is destroyed due to the energy bias, and, furthermore, the states are well localized. Near the barrier top, where tunnel splitting occurs in a symmetric potential, the wave functions assume finite values in the adjacent wells, and, therefore, the probability of surviving in the initial well is reduced due to incoherent tunnelling. The wave functions above the barrier top are not much affected by the energy bias and resemble the corresponding wave functions of the symmetric case.

The symmetric potential, represented in figure 1, was used to argue that OH^- impurities in $LiNbO_3$ do not form hydrogen bonds, because, from experimental evidence, localized proton states must be assumed in this system, and, furthermore, the observed transition frequencies are at variance with the energy levels and tunnel splittings of this traditional DMP [15]. Referring to hydrogen bonds in general, however, this argument is not completely conclusive, because at least the prediction of delocalized states in the DMP model could be amended by the introduction of an energy bias according to figure 2, and

there is growing experimental evidence that the idea of a universal DMP model, though frequently adopted, is not a completely satisfactory description of hydrogen bonds.

Table 1. Different sets of parameters of double Morse potentials, describing hydrogen bonds in different materials, and the extrapolated free-stretching frequencies. The parameters of reference [2] are also used in, e.g., references [8] and [9]. The parameters of reference [15] have been used for the calculations of figure 1.

Reference	u_{M0} (eV)	a (nm^{-1})	ν_∞ (cm^{-1})
[2]	5.34	28	4638
[3]	1.18	49.5	3210
[5]	1.44	45.3	3397
[6]	2.94	46.8	5315
[15]	2.36	40	4098

If one compares the DMP parameters which have been used in the literature (table 1), it can be noticed that these parameters differ considerably. Furthermore, if the presupposition of a universal DMP was correct, this potential should give, at least approximately, the frequency of the free proton stretching mode ν_∞ in the limit $R \to \infty$, observed, e.g., in gaseous CH_3COOH at 3583 cm^{-1} [11], or in isolated HDO molecules at 3707 cm^{-1} [29]. None of the frequencies predicted from the different sets of parameters (table 1) is in reasonable agreement with these experimental frequencies. In fact, it must be concluded that a DMP in connection with a certain set of parameters is only valid for a limited range of the bond length R, and may be useful for the comparison of proton and deuteron states in a specific material [3–6].

The Morse function, describing a single-well potential, may be written in the form

$$u_M(r) = u_{M0}\{\exp[-2a(r-r_0)] - 2\exp[-a(r-r_0)]\}. \tag{2}$$

In this function, a is a strength parameter and u_{M0} stands for the depth of the potential. In connection with hydrogen bonds, the equilibrium distance in OH^- ions $r_0 = 96$ pm is generally adopted. The energy levels in the potentials of figure 1 or figure 2 are inconsistent with the observed transition frequencies, because the barriers are too low. In particular, the third excited state is in the vicinity of the barrier top, and shows a tunnel splitting of 314 cm^{-1}, which was not observed. Mathematically speaking, the low barrier of a DMP is caused by the long-range attractive part of the function $u_M(r)$, characterized by the parameter a, which is one half of the repulsive parameter $b = 2a$. Therefore, one may think of a different form $u(r)$, which has an attractive part of shorter range, and an additional parameter is needed to decouple the repulsive and attractive parts of the potential. The obvious generalization of the Morse potential (equation (2)) along these lines is

$$u(r) = u_0\left\{\frac{a}{b-a}\exp[-b(r-r_0)] - \frac{b}{b-a}\exp[-a(r-r_0)]\right\}. \tag{3}$$

In this form, however, the attractive parameter a is not totally decoupled from the repulsive parameter b, because the relation $b > a$ must be fulfilled. In the case where $b < a$, the two terms just exchange their meanings, the attractive part becoming the repulsive part, and vice versa. Another shortcoming of this form is the fact that the case $a = b$ must be excluded.

In this work, a generalization of the Morse potential is assumed, which is not obvious

at first sight:

$$u(r) = u_0 \frac{a\,\{\exp[-b(r-r_0)]-1\} + b\,\{\exp[a(r-r_0)]-1\}}{a + b\exp[a(r-r_0)]} - u_0. \qquad (4)$$

This form was obtained by the combination of independent repulsive and attractive parts, and a step function, which switches between these parts at $r = r_0$, the position of the minimum. The parameters a and b control the shape of the potential for $r > r_0$ and $r < r_0$, respectively. It can be easily shown that for $b = 2a$ equation (4) is equal to the Morse function (equation (2)).

The proton potential of an OH^- ion in a crystal is determined, in a first approximation, by the intra-ionic bond to the oxygen. In many cases, other interactions make only a minor contribution, which can be concluded from 'typical' stretching frequencies in the range ~3500–3700 cm^{-1}. Additional neighbouring oxygen atoms are of particular importance, because of the possible building of hydrogen bridges. Depending on its distance to the OH^- ion, an oxygen atom has an increasing influence with decreasing separation, which becomes apparent in the experimentally observed frequency–bond-length correlation [11]. For large distances, the influence of a neighbouring oxygen is accordingly weak and competes with other solid-state phenomena like, e.g., dielectric properties or proton–proton interaction. Whether or not an H bridge is built in these cases can experimentally be decided only by the determination of the proton position (e.g., by neutron diffraction). $OH:LiNbO_3$ certainly represents one of these borderline cases, for which the question concerning hydrogen bonding is a subject of controversy in the literature.

Table 2. Experimental transition frequencies ν_{exp} in proton-exchanged (p) and deuteron-exchanged (d) $LiNbO_3$ and the respective linewidths $\Delta\nu$ [15]. The theoretical values ν_{calc} have been calculated using the following two parameter sets. Set I: $u_0 = 3.015$ eV, $a = 105$ nm^{-1}, $b = 15.2$ nm^{-1}, $R = 308$ pm. Set II: $u_0 = 3.350$ eV, $a = 71.0$ nm^{-1}, $b = 20.0$ nm^{-1}, $R = 288$ pm. For the proton and deuteron reduced masses the values $\mu_p = 0.9412 m_p$ and $\mu_d = 1.7778 m_p$ have been assumed. In the last column, the calculated tunnel splittings Δ of the excited states (set II) are listed. For set I, the tunnel splittings are fractions of a wavenumber in every case. The 'free'-stretching frequency for set II is $\nu_\infty = 3577$ cm^{-1}.

	ν_{exp} (cm^{-1})	$\Delta\nu$ (cm^{-1}) (FWHM)	ν_{calc} (cm^{-1}) Set I	ν_{calc} (cm^{-1}) Set II	Δ (cm^{-1})
$0 \rightarrow 1$ (d)	2588(2)	21	2592	2582	0.000
$0 \rightarrow 1$ (p)	3508(2)	30	3507	3505	0.015
$0 \rightarrow 2$ (d)	5084(4)	46	5081	5080	0.001
$0 \rightarrow 2$ (p)	6836(4)	67	6830	6843	0.52
$0 \rightarrow 3$ (d)	7487(8)	65	7476	7485	0.028
$0 \rightarrow 4$ (d)	9783(12)	85	9783	9783	0.65
$0 \rightarrow 3$ (p)	9989(8)	127	9986	9978	11
$0 \rightarrow 4$ (p)	12 965(16)	170	12 975	12 827	150

In the present paper the following approximations have been adopted.

(i) The proton–oxygen interaction due to the covalent bond within the OH^- ion is described by an energy function $u(r)$ with a single minimum at $r_0 = 96$ pm.

(ii) The interaction with a second oxygen atom is taken into account by the same function $u(-r - R)$.

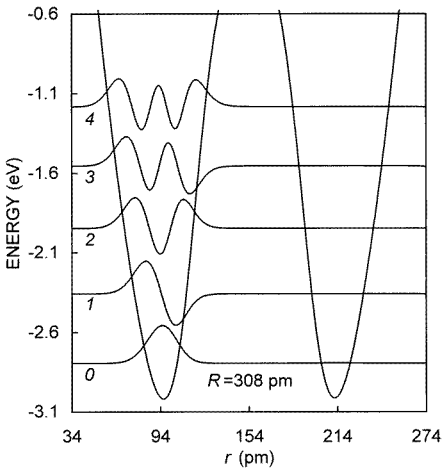

Figure 3. Wave functions of proton states in the left-hand well of the present model potential for a bond length $R = 308$ pm, using parameter set I. The baselines of the wave functions correspond to the energies given in table 2.

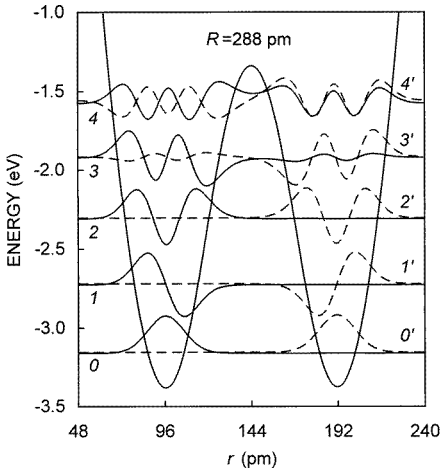

Figure 4. Wave functions of proton states in the double-well potential of the present model for a bond length $R = 288$ pm, using parameter set II. The baselines of the wave functions correspond to the energies given in table 2.

These two assumptions (i) and (ii) are analogous to the DMP model, except that the Morse function (2) is replaced by equation (4).

(iii) In contrast to the DMP model, the most frequent case $X_1 \neq X_2$ is taken into account by an asymmetry factor $U(r) = cu(r) + c^{-1}u(-r - R)$. Generally, there is only little information about an energy bias available. Therefore, the asymmetry factor is fixed at a value of $c = 1.001$ here, which is sufficient for the localization of the states, but hardly noticeable, e.g., in figure 3.

For the determination of the proton potential, a case is favourable where (a) the environmental influence on the OH^- ion is weak, and (b) as many as possible of the transition frequencies have been determined. For a parameter set I, the model potential has been applied to the OH:$LiNbO_3$ system, because it fulfils the above-mentioned requirements, and the negative mode-Grüneisen parameter has not been understood yet. For the bond length, a value of $R = 308$ pm was assumed, and the parameters a, b and u_0 were fitted to the observed frequencies. For the reduced masses, the values $\mu_p = 0.9412m_p$ and $\mu_d = 1.7778m_p$ have been used [30]. Table 2 presents the comparison of the experimental and theoretical frequencies for both proton and deuteron stretching frequencies. It can be noticed that the experimental frequencies are reproduced within experimental accuracy. Figure 3 shows a representation of this model potential I and the respective proton states of the left-hand well, which are well localized. This potential shows that the experimental evidence concerning localized proton states and energy levels in OH:$LiNbO_3$ is not in contradiction to the possible existence of a double-well potential.

For hydrogen bonds in other substances, however, this model potential I does not sufficiently reproduce the $\nu(R)$ correlation. For a second parameter set II, a value of $R = 288$ pm was assumed, and the parameters were fitted with the additional requirement of reproducing the proton stretching frequencies at around $R = 250$ pm [11], maintaining as much of the overtone spectrum as possible. The predicted frequencies of this model II

are also given in table 2, together with the calculated tunnel splittings of the excited levels. The potential and the quantum states are represented in figure 4. It can be observed that the transition frequencies are still well reproduced, except the third proton overtone.

In section 3, the quantum states of this model potential II will be presented for different values of the bond length R. The predictions of this model for the fundamental transition frequency, as well as line intensities and linewidths, will be discussed in comparison to the results of optical experiments on real systems with corresponding bond lengths.

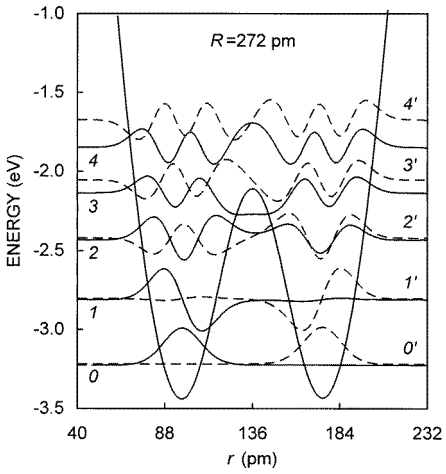

Figure 5. Wave functions of proton states in the double-well potential of the present model (parameter set II) for a bond length $R = 272$ pm.

3. Examples

In $MgSO_4 \cdot 6H_2O$ a bond length of $R = 272$ pm is observed, and the observed frequency is 3320 cm^{-1} [11]. The hydrogen bonds in H_3BO_3 have the same bond length, but the frequency of 3200 cm^{-1} is somewhat lower [11]. For the uncoupled OH modes in amorphous D_2O under pressure, a value of 3200 cm^{-1} was obtained for a bond length of about 270 pm [31]. For $R = 272$ pm, the model predicts a transition frequency of 3348 cm^{-1} (figure 5).

Figure 6 illustrates the situation when the first excited states are energetically in the vicinity of the barrier top. Here, their wave functions assume finite values in the opposite wells, because the tunnel splitting becomes comparable to the energy bias. There is a certain probability that the protons escape from the initial well during an excitation process, and, therefore, lifetime broadening must be attributed to these excited levels. The spectra of CH_3COOH crystals at 90 K, in which the H bonds have a length of 262.5 pm, do indeed show a rather broad peak at 2875 cm^{-1} [11]. The calculated transition frequency is somewhat higher. In compressed ice, a bond length of 264 pm corresponds to a pressure of about 26 GPa. Raman and IR measurements showed a substantial line broadening in this range, and the lines of the proton stretching modes were no longer detectable at higher pressures [24–26].

For a bond length of $R = 256$ pm (figure 7), state 1 is very close to the barrier top, while $1'$ lies considerably higher. The four possible transitions between the two ground

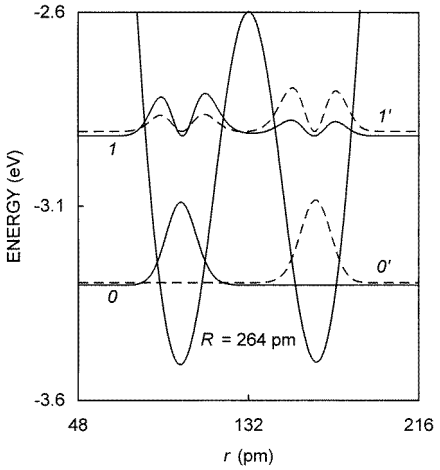

Figure 6. Squares of the wave functions of the ground and first excited states for a bond length of $R = 264$ pm (set II). In this bond-length regime, the states 1 and $1'$ have finite probabilities in the adjacent wells, and lifetime broadening has therefore to be expected for the corresponding transitions. The 01 transition frequency is 3103 cm^{-1}.

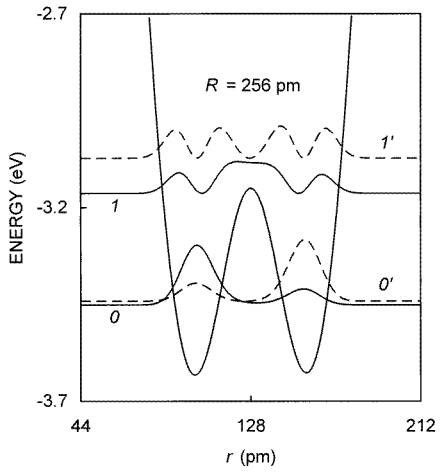

Figure 7. Squares of the wave functions of the four lowest states for a bond length of $R = 256$ pm. The potential parameters are the same as in the preceding figures. The situation is quite close to that of the hydrogen bonds in $NaHCO_3$ or $(CH_3)_2AsOOH$ (see the text).

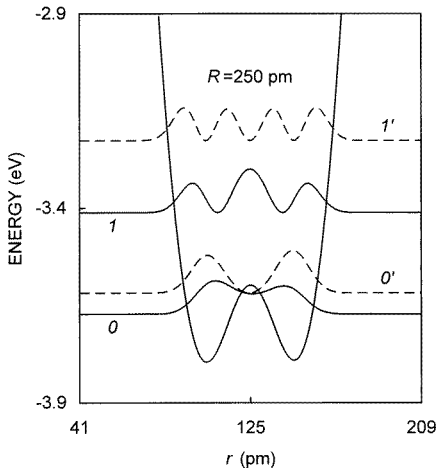

Figure 8. The four lowest states for a bond length of $R = 250$ pm. The potential parameters are the same as in the preceding figures. A similar potential has been obtained using the DMP model with parameters specially adapted to describe the transition frequencies in CrOOH and CoOOH [5] (see table 3).

states and the two excited states have frequencies of 2245 cm^{-1}, 2322 cm^{-1}, 2979 cm^{-1} and 3056 cm^{-1}. Raman spectra of $NaHCO_3$ (bond length 259 pm) show a complex band with four lines at 2430 cm^{-1}, 2530 cm^{-1}, 2910 cm^{-1} and 3050 cm^{-1} [11]. There is, of course, no exact agreement between the transition frequencies of the present model and the observed frequencies in $NaHCO_3$; however, the prediction of two doublets in this bond-length regime is in excellent qualitative agreement with the experimental results. Similar

arguments apply to the interpretation of the Raman spectra of $(CH_3)_2AsOOH$ (bond length 257 pm). The spectra are again dominated by two doublets, shifted to lower wavenumbers and with considerably larger linewidths [11].

In this bond-length regime, the two ground states 0 and 0′ assume finite values in the opposite wells, because the energy of the tunnel splitting becomes comparable to the energy bias. The model potential now achieves the characteristics of a two-level system (TLS). The TLS model is used to describe the properties of amorphous substances [32], and has also been applied to the problem of proton transfer at low temperatures [28]. Due to the low barrier, the occurrence of disorder must be expected in real systems, even at low temperatures. From Raman spectra of the lattice modes in H_2O ice it was concluded that this substance transforms from the ordered polytype ice VIII to the disordered form ice VII at about 60 GPa ($R \approx 247$ pm) in the vicinity of the absolute zero of temperature [33], and not to the proposed symmetric ice X.

Table 3. Transition frequencies in chromous and cobaltic acid [5] (a: experimental; b: theoretical), and the frequencies of the present model II for $R = 250$ pm (c). The intensity ratios obtained according to equation (A4), using the wave functions illustrated in figure 8, are also given.

	ν_{ij} (cm^{-1})					
	CrOOH		CoOOH			
	a	b	a	b	c	I_{ij}/I_{01}
$0 \rightarrow 0'$	518	214	221	202	436	59
$0' \rightarrow 1$	1650	1621	1800	1667	1655	131
$0 \rightarrow 1$					2091	1
$0 \rightarrow 1'$	3400	3264	3450	3338	3581	15

Figure 8 illustrates the model potential and the squares of the wave functions of the four lowest energy levels for $R = 250$ pm. The splitting of the ground states is considerably increased, which means that the fundamental transition, i.e. the proton stretching mode, changes its character in this regime. The model predicts the highest intensity (see the appendix) for the 0′1 transition, while the intensity for the 01 transition, which is the fundamental transition in weak H bonds, is negligible (table 3). In chromous acid CrOOH (bond length 249 pm) and cobaltic acid CoOOH (bond length 250 pm), the H bonds are quite close to the situation in figure 8 [5]. These substances have been the subject of a theoretical investigation using a DMP in the WKB approximation [3, 5]. From their calculations the authors propose an assignment for the observed IR frequencies, which is given in table 3, together with their best values and the results of the present model. Although the parameters of the present model have not been specially adapted, the agreement between the experimental and model frequencies is quite close.

At this point it is interesting to have a brief look at the predictions of the present model when the proton reduced mass is replaced by the deuteron reduced mass $\mu_d = 1.7778 m_p$ [30]. In CrOOD and CoOOD the bond lengths depend quite strongly on deuteration, and the OO distance is increased to about 256 pm. In reference [5] it has been pointed out that the doublet observed in the IR spectra of these substances (1620 and 1940 cm^{-1}, approximately) can be well represented by replacing just the different bond lengths and the masses. In the present model the 01 (1944 cm^{-1}) and 0′1′ (2092 cm^{-1}) transition frequencies are somewhat

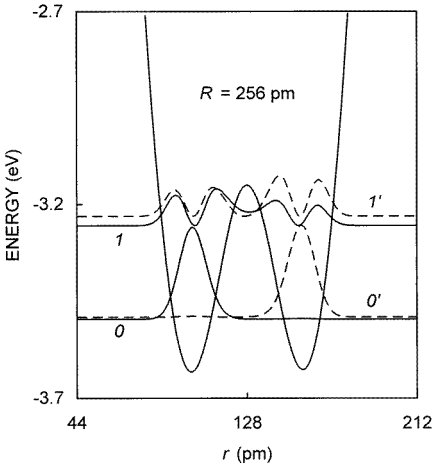

Figure 9. Deuteron states for a bond length of $R = 256$ pm. The potential parameters are the same as in the preceding figures (see also figure 7), but the proton reduced mass has been replaced by the deuteron reduced mass $\mu_d = 1.7778 m_p$. The situation corresponds to the hydrogen bonds in CrOOD and CoOOD [5].

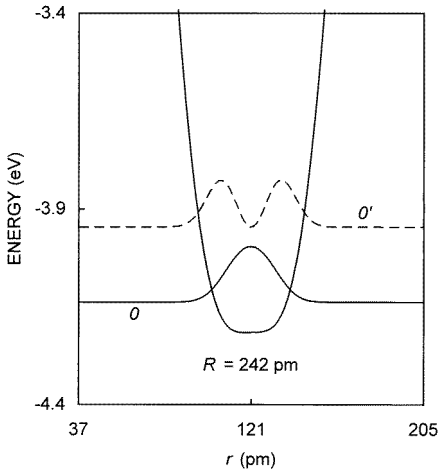

Figure 10. The present model potential becomes symmetric at about 242 pm. The transition frequency is 1552 cm^{-1}.

larger, but a similar doublet is predicted. Figure 9 shows a representation of the potential and the squares of the wave functions.

The present potential becomes symmetric at about 242 pm (figure 10). It can be noted that the second derivative, i.e. the force constant of the classical motion, vanishes at the centre of the bond, while the frequency of the transition between the two quantum states is 1552 cm^{-1}. The potential is rather anharmonic, and a strong coupling to the normal modes of the environment can therefore be expected in real systems. Furthermore, the maximum of the ground-state wave function is much more extended than in the non-symmetric case (see, e.g., figure 6), which means that the proton position is not very well defined.

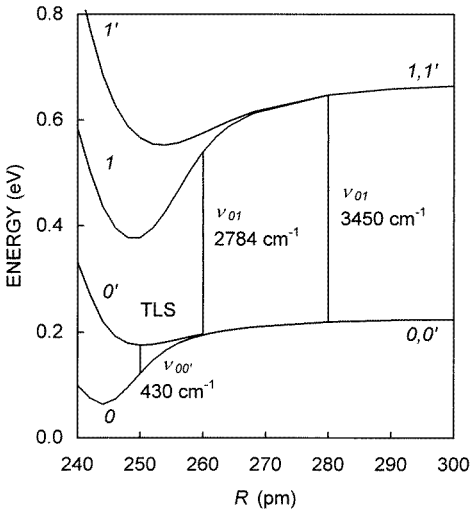

Figure 11. Energy differences between the energy levels and the bottom of the respective wells. Some selected transition frequencies are also given. In the TLS (two-level system) regime, the barrier is of the order of the ground-state energies. Here the ground states split, giving rise to the new fundamental transition $00'$ of symmetric H bonds.

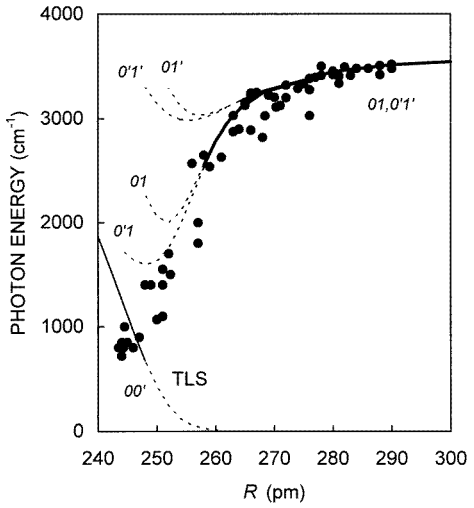

Figure 12. Proton-transition frequencies for different values of the bond length R of the present model and the data of reference [11] (circles).

The results of the present calculations for the energy levels and the transition frequencies are summarized in the following figures and compared to the experimental frequency–bond-length correlation. Figure 11 shows the evolution of the energy levels relative to the bottom of the respective well. For weak H bonds ($R > 270$ pm), the energy levels in the two wells are almost degenerate, and the 01 and $0'1'$ transition frequencies slowly decrease with decreasing bond length. For intermediate H bonds (260 pm $< R <$ 270 pm), the degeneracy of the 1 and $1'$ states is removed in the vicinity of the barrier top (see also figure 6), and the 01

frequency decreases more strongly, which causes a knee-shaped curvature in the frequency–bond-length correlation (figure 12). The transition 01, which corresponds to the fundamental proton stretching frequency of weak H bonds, actually exhibits a minimum somewhere around $R = 250$ pm, as has been assumed to be the indication for the symmetrization of the bond; this minimum, however, is in the TLS regime, where the ground state has already split into 0 and 0′, and therefore 00′ has become the fundamental transition, while 01 is the first overtone.

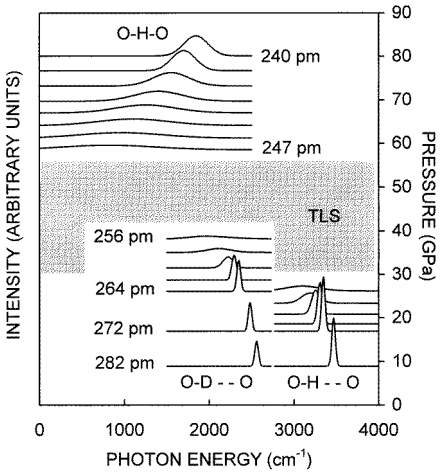

Figure 13. Calculated transition lines (equation (A3)) for different values of the bond length R. The pressure scale corresponds to the equation of state of ice [34]. The shaded area represents the TLS regime, in which sharp optical transitions are not to be expected. The curves in the upper third of the figure represent lines in symmetric bridges (see figure 10) with a linearly decreasing linewidth.

By means of equation (A3) of the appendix, optical transition lines can be simulated. In the range of weak H bonds, the intensities increase with decreasing R mainly due to the reduction of the volume, and the transition-matrix element plays only a minor role, being almost constant, as long as there is no great degree of tunnelling of the states (figure 13). The transition lines of the proton modes become considerably broader below about $R = 270$ pm. At about $R = 264$ pm, which corresponds to $p \approx 27$ GPa in compressed ice, the width of the lines is so large that the lines would be hardly observable in an optical experiment, using the diamond-anvil technique. This limiting pressure is in very good agreement with the line broadenings and the ultimate disappearance of the lines observed in ice [24–26]. For deuteron modes, the respective broadenings take place at considerably shorter bond lengths (or higher pressures), which again is in excellent agreement with the experimental findings [25].

In the upper third of figure 13, calculated lines for the 00′ transitions in symmetric bonds are shown. Here the linewidths can be assumed to be caused by a strong anharmonic coupling to environmental modes, which is reduced as the potential becomes more and more harmonic. Therefore, the linewidths have been assumed to decrease linearly with decreasing bond length in these calculations (linewidths cannot be defined analogously to equation (A2) for transitions in single-minimum potentials). The matrix element is larger by a factor of two than for the transitions in the double-well regime, and the intensity of the lines is furthermore increased, because of volume reduction. Thus, the predicted lines

are quite strong, which is in good agreement with IR spectra for $NaH(CH_3COO)_2$ crystals, with a bond length of 244 pm [11].

4. Discussion

Because of its approximate character according to (i)–(iii) of section 2, model II can be regarded as an approach to the case of dilute hydrogen bonds in solids, with weak interactions to their environment. In real systems, such interactions may cause differences in the proton stretching frequency within a range of about 100–200 cm^{-1} [11]. However, in comparison to the traditional DMP model, the description of optical transitions in hydrogen bonds is considerably improved by the present model, which has been demonstrated in the foregoing section. On the one hand, this improvement is related to the asymmetry of the potential, which makes it possible to account for the fact that proton states in weak hydrogen bonds are localized. Conceptual difficulties in connection with theoretically predicted delocalized states in symmetric potentials are thereby avoided, and the observed line broadenings in intermediate and strong hydrogen bonds can be linked to lifetime broadening. On the other hand, this improvement must be seen in connection with the use of equation (4). This form makes it possible to construct double-well potentials at around $R = 300$ pm with only weak anharmonicity over several excited states, and to represent also the frequency–bond-length correlation in intermediate and strong hydrogen bonds without a change of parameters.

For weak hydrogen bonds, the interaction of the proton with its second-nearest-neighbour oxygen atom is much smaller in the present approach than in the traditional DMP model. The fact that the influence of the second oxygen in weak hydrogen bonds is overestimated in the DMP model finds more direct support in the results of a neutron diffraction study on compressed ice, which revealed a much weaker pressure dependence of the OH^- bond length, $dr_{OH}/dp = 0.04(4)$ pm GPa^{-1} [16], than previously estimated on the basis of the DMP model, $dr_{OH}/dp = 0.2$ pm GPa^{-1} [2, 35]. For the present model II, the variation of r_{OH} with the bond length R at around $R = 300$ pm is in excellent agreement with these experimental findings, because it predicts a value of $dr_{OH}/dR = -0.016$. Using the equation of state of ice [34], this value corresponds to $dr_{OH}/dp = 0.04$ pm GPa^{-1}, which obviously corresponds to the value of reference [16] within the experimental accuracy.

In conclusion, the present model potential is experimentally indistinguishable from a single-minimum potential for weak hydrogen bonds, and the influence of the second-oxygen-neighbour atom is rather weak, competing with other solid-state interactions, which are neglected in the present approach. With regard to the $OH:LiNbO_3$ system, whose overtone spectrum has been used here for the determination of the potential, this means that there is no experimental evidence as to whether or not hydrogen bonds are built in ambient conditions, although the observed negative mode-Grüneisen parameter [17] points in this direction. However, the differences between the two parameter sets I and II may also be interpreted in such a way that the model II is not optimal for this system. These questions will be discussed more thoroughly in a forthcoming paper [36].

The phenomenological classification of hydrogen bonds [11] finds support in the present calculations. In weak hydrogen bonds, the ground and first excited states are well localized and sharp transition lines can be expected. In intermediate bonds, the first excited state is near the barrier top and is affected by lifetime broadening. The frequency–bond-length correlation adopts a steeper decrease in this range at the same time. Strong hydrogen bonds have only a low barrier or are symmetric.

The DMP model was used to predict symmetrization of hydrogen bridges in ice under

strong compression [2, 8, 14]. However, the use of the DMP model is questionable because of its shortcomings, discussed in the foregoing sections. Using the present model, the results for the transition frequencies are represented in the upper third of figure 13. At present, there is considerable activity in IR experiments on ice, because the MIR range has become accessible to high-pressure experiments at pressures above 100 GPa only recently [24, 26, 37, 38]. But, at first sight, the results of these most recent experiments do not reveal clear evidence for a proton stretching mode of symmetric bonds, according to figure 13.

IR measurements on ice films in Xe as the pressure-transmitting medium up to 85 GPa show first of all an enormous broadening of the fundamental ice stretching peak at low pressures, completely analogous to the observations in Raman experiments [25]. At the ultimate pressures of these experiments on H_2O:Xe, no evidence for absorption due to a proton stretching mode in ice can be observed. The only spectral feature which is present in these spectra has been assigned by the authors to a librational mode in ice (or distortional mode ν_D in reference [26]). The authors note an asymmetric peak shape and explain this shape as a Fano resonance of the respective mode with a stretching continuum.

Spectra of H_2O:KBr samples (ice films with KBr as the pressure medium) are somewhat different from the H_2O:Xe spectra: the asymmetry of the ν_D-peak is smaller, but its intensity is considerably increased at higher pressures [26]. Furthermore, a new (symmetric) peak appears at low wavenumbers and is completely resolved at a pressure of 112 GPa. This new peak was assigned to a translational mode ν_T of ice [26].

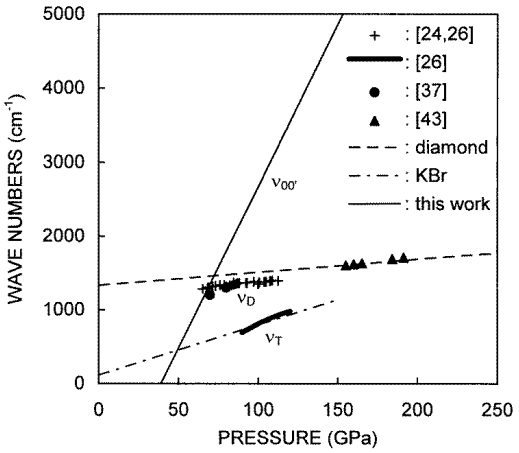

Figure 14. Results of recent IR experiments at very strong compression and the frequency of the $00'$ transition of the present model (continuous line). ν_D has been assigned by the authors to a distortional mode in H_2O:Xe and H_2O:KBr [24, 26], and ν_T to a translational mode in H_2O:KBr [26]. Triangles represent absorption peaks, which have been assigned to a new lattice mode in H_2 [43]. Circles stand for intersections between bands in reflection spectra of H_2O [37]. The dashed line represents the pressure shift of the optical phonon in strained diamond anvils from Raman measurements [39]. The chain line denotes the extrapolation of the TO-phonon frequency of KBr, according to its mode-Grüneisen parameter and the equation of state of KBr [41, 42].

Figure 14 presents the calculated pressure dependence of the $00'$ transition and the observed peak positions of references [24, 26]. It can be observed that the experimental frequencies show a much weaker pressure dependence than one would expect for ice modes, according to the present calculations. Instead, ν_D shows a spectral position and pressure

shift which are almost identical to the behaviour of the optical phonon in strained diamond anvils, according to the Raman measurements of reference [39]. The tips of diamond anvils are strongly strained in a high-pressure experiment, giving rise to distorted Raman spectra of the optical phonon [40]. One may thus speculate that the selection rules are broken in strained diamond anvils, giving rise to IR activity of the optical phonon. In particular, this would explain the increasing intensity of the ν_D-peak with increasing load.

In reference [26], KBr has been used as the pressure medium, which actually means that most of the sample chamber was filled with this material. The optical phonon in KBr is IR active, but IR spectra of KBr have not been taken in this pressure range. However, from the position of the optical phonon of KBr in ambient conditions and its mode-Grüneisen parameter [41], using the equation of state of KBr [42] and accounting for the phase transition of this material at 2 GPa, one may estimate the position of the optical phonon of KBr in the pressure range in question (figure 14). It can be noted that this extrapolated frequency coincides almost exactly with the position and shift of the ν_T-peak of reference [26]. It is therefore not completely unlikely that the ν_T-peak is attributable to KBr, and not to ice.

Most recently, reflection measurements on ice up to 210 GPa have been reported [37, 38]. The original spectra at 69.7 GPa and 80.0 GPa of reference [37] seem to show two broad reflection bands below 2500 cm^{-1}, and have been accordingly assigned. However, the intersection of these bands occurs at around 1300 cm^{-1}, again in the range of the diamond phonon (figure 14). In view of the aforementioned possibility of optical activity in the diamonds, one might interpret these spectra as a single reflection band, obscured by absorption in the diamond anvils.

Regarding this unclear situation about the assignment of spectral features in experiments using the diamond-anvil technique, an independent experiment for the same pressure range would be useful, and such an experiment has actually been performed in reference [43]. The authors present IR absorption measurement on hydrogen up to 191 GPa, and find a peak in a spectral range where no modes in hydrogen have been reported before. Therefore, this peak has been assigned to a 'new' lattice mode of hydrogen [43]. Figure 14 shows also the respective peak positions of reference [43], and it can be noted that the frequency and pressure dependence coincides almost exactly with the behaviour of the diamond phonon. Furthermore, the intensity of this new peak increases with increasing pressure, thus showing the same characteristics as the ν_D-peak of reference [24] and [26].

At ambient conditions, absorption in diamond anvils due to two- and three-phonon processes between 1800 cm^{-1} and 4000 cm^{-1} is well known [44], but IR measurements in this frequency range at pressures of 100 GPa and above are relatively new. The measurements of references [24, 26, 37, 43] with rather different contents of the diamond-anvil cells have a spectral feature in common, which (1) has the frequency of one-phonon processes in diamond, (2) shows the same pressure dependence and (3) increases in intensity with increasing load. A possible artificial signal from the diamond anvils must therefore be taken into consideration.

Disregarding the possible absorption in the diamonds, there is a good chance that a signal from transitions in symmetric bonds in ice has been observed in the reflection measurements of reference [37]. The spectra at 69.7 GPa and 80.0 GPa show a broad band in the low-frequency range, reaching up to about 2500 cm^{-1}. This is the pressure range where the calculated $\nu_{00'}$-transition crosses the diamond line in figure 14, and spectra of this type (but without a dip at 1300 cm^{-1}) are what one would actually expect in reflection measurements. Unfortunately, no original spectra at higher pressures are given in reference [37], although the experiments were performed up to 210 GPa.

However, it may be possible that the predicted frequency shift of the $\nu_{00'}$-transition in figure 14 will not be observable above 100 GPa, because such pressures correspond to bond lengths considerably shorter than 240 pm, and such short hydrogen bonds have not been observed in substances in ambient conditions. A simple one-dimensional model may not be appropriate for such short oxygen distances, and one may have to take into account a multi-dimensional energy surface with a saddle point at the bond centre and an average proton position away from this centre.

In future IR experiments, using the diamond-anvil technique at pressures around 100 GPa and above, the possible IR activity of the diamond anvils around 1300 cm^{-1} has to be clarified and eventually excluded from the interpretation of the spectra. For experiments on ice in this pressure range, figures 13 and 14 may serve as a guide, where transitions in symmetric bonds have to be expected.

Acknowledgment

I thank W B Holzapfel for many fruitful discussions.

Appendix

By means of the Numerov (Fox–Goodwin) algorithm, the second-order differential equation (1) is solved by a two-step recursion [45]:

$$\Psi_{i+2} = \frac{2\Psi_{i+1} - \Psi_i - (\delta^2/12)(10F_{i+1}\Psi_{i+1} + F_i\Psi_i)}{1 + (\delta^2/12)F_{i+1}} + O(\delta^6) \tag{A1}$$

with the step width δ, and $\Psi_i \equiv \Psi(i\delta)$, $F_i \equiv F(i\delta)$, and

$$F(r) = \frac{2\mu}{\hbar^2}[E - U(r)].$$

In all the calculations, presented in the foregoing sections, a step width of $\delta = 1$ pm was used. For the start of the recursion (equation (A1)), two values of the wave function at $r = 0$ and $r = \delta$ are required. The determination of these start values depends on the respective problem, to which the algorithm is to be applied. In case of a symmetric potential $U(-r) = U(r)$, the wave functions are alternately symmetric and anti-symmetric, $\Psi(-r) = \pm\Psi(r)$, with increasing energy. For anti-symmetric functions, one has $\Psi(0) = 0$. For $\Psi(\delta)$ an arbitrary value $\Psi(\delta) \neq 0$ can be used, which may be determined by a normalization condition. The start values for symmetric functions are a bit more complicated [45], but of no interest here.

In the present study, non-symmetric double-well potentials for $r \geqslant 0$ are considered. These can be easily symmetrized by a reflection at $r = 0$. Thus, symmetric four-well potentials with doubly degenerate energy levels are in fact considered. The solutions of the wave functions for $r < 0$, however, are not physically relevant.

The eigenvalues of the energy E_i are those values for which the wave functions $\Psi_i(r)$ vanish in the limit $\lim_{r\to\infty} \Psi_i(r) = 0$. This condition can be fulfilled numerically only approximately by the condition that the wave functions vanish in a region which lies sufficiently outside the turning points of the classical motion.

For a given potential, the wave functions and eigenvalues can be readily computed, but for fitting purposes, e.g., the determination of model parameters from experimental transition energies, the algorithm is not very well suited. Thus, in the present case, the potential parameters have been determined using approximate WKB energies in a first step.

The squares of the wave functions of the energy levels which are far below the barrier top of a non-symmetric double-well potential exhibit finite values in either one of the wells. For normalized wave functions the integral

$$q_i = \int_0^{R/2} |\Psi_i(r)|^2 \, \mathrm{d}r \tag{A2}$$

calculated for one half of the double-well potential is unity in such a case, while the integral calculated for the other half of the potential is zero. For energy levels, which are sufficiently near the barrier top, q_i is no longer unity, and the integral for the opposite well also assumes finite values. In such cases, q_i can be interpreted as the probability for the proton to survive in the well, and a respective width $\sigma_i = -E_i \ln q_i$ can be attributed to the energy level. For an optical transition one has consequently the linewidth $\sigma_{ij} = \sigma_0 + \sigma_i + \sigma_j$, with some intrinsic width σ_0 [46], and the widths of the initial σ_i and the final state σ_j. Using a Gaussian profile, a transition line can be represented by

$$I(E) = \frac{I_{ij}}{\sigma_{ij}\sqrt{2\pi}} \exp\left[-\frac{(E_{ij} - E)^2}{2\sigma_{ij}^2}\right]. \tag{A3}$$

With the help of the wave functions, the transition intensities I_{ij} can be calculated [47]:

$$I_{ij} = CNE_{ij} \left|P_{ij}\right|^2. \tag{A4}$$

Here C is a proportionality constant, N stands for the number of oscillators per volume, E_{ij} is the transition energy and P_{ij} represents the transition matrix element:

$$P_{ij} = \int_0^{\infty} \Psi_i(r)\mu(r)\Psi_j(r) \, \mathrm{d}r \tag{A5}$$

with the dipole-moment function $\mu(r)$.

Table A1. Intensity ratios of the optical transitions in PE and DE $LiNbO_3$ [15] (superscript a). The calculated values of reference [15] are based on the wave functions of a single-oscillator model and the assumption of a fourth-order polynomial for the dipole-moment function. For the values of the present work (superscript b), the wave functions, which are illustrated in figure 4, have been used together with a second-order polynomial for the dipole-moment function (see the text).

	Experimental[a]	Calculated[a]	Calculated[b]
I_{01}/I_{02}(OH)	165	166	165
I_{02}/I_{03}(OH)	16	16	12
I_{03}/I_{04}(OH)	8	8	78
I_{01}/I_{02}(OD)	175	228	176
I_{02}/I_{03}(OD)	22	21	28
I_{03}/I_{04}(OD)	15	11	18

By means of equations (A4) and (A5) transition intensities can be calculated when the dipole-moment function is known. Different forms of the dipole-moment function have been tested, taking again the $LiNbO_3$ system as an example case. Reasonable agreement between the observed and calculated intensities could be obtained (table 4) using a second-order polynomial $\mu(r) = \mu_1 r + \mu_2 r^2$, with $\mu_2/\mu_1 = -20$ nm^{-1}, except again for the highest proton overtone.

The proposed potential equation (4) is extremely flexible, which may also be suitable for other applications. In the extreme case $a \gg b$, the function approximates a step function,

with $u(r) \approx -u_0$, for $r < r_0$, and $u(r) \approx 0$, for $r > r_0$ (the approximation means here that the function remains analytical). In the other extreme case $a \ll b$, the function is almost constant $u(r) \approx -u_0$, for $r > r_0$, and adopts very large values for $r < r_0$, thus approximating a 'hard-sphere' potential. Between these limiting cases, the function adopts more common forms, being identical to the Morse function for $b = 2a$. In a double-minimum potential, these properties of equation (4) mean that the form of such a double-minimum potential can continuously be varied from an almost rectangular barrier ($a \gg b$, $u(r) \approx 0$, for $r_0 < r < R - r_0$, and $u(r) \approx -u_0$, elsewhere) through 'usual' types of double-minimum potentials (e.g., $b = 2a$, the double Morse potential), to, finally, an almost rectangular well in the other limiting case ($a \ll b$, $u(r) \approx -2u_0$, $r_0 < r < R - r_0$, and $u(r) \to \infty$, elsewhere).

References

[1] There are different ways to define a double Morse potential. The definition given here has been somewhat simplified for convenience.

[2] Holzapfel W B 1972 *J. Chem. Phys.* **56** 712

[3] Lawrence M C and Robertson G N 1980 *Ferroelectrics* **25** 363

[4] Lawrence M C and Robertson G N 1980 *J. Phys. C: Solid State Phys.* **13** L1053

[5] Lawrence M C and Robertson G N 1981 *Mol. Phys.* **43** 193 and references therein

[6] Lawrence M C and Robertson G N 1981 *Ferroelectrics* **34** 179

[7] Matsushita E and Matsubara T 1982 *Prog. Theor. Phys.* **67** 1

[8] Schweizer K S and Stillinger F H 1984 *J. Chem. Phys.* **80** 1230

[9] Mackowiak M 1987 *Physica* B **145** 320

[10] Mackowiak M 1989 *J. Mol. Struct.* **192** 189

[11] Novak A 1974 *Struct. Bonding* **18** 177 and references therein

[12] Krobok M P, Johannsen P G and Holzapfel W B 1992 *J. Phys.: Condens. Matter* **4** 8141

[13] Hamilton W C 1968 *Hydrogen Bonding in Solids* (New York: Benjamin)

[14] In connection with hydrogen bonds and double-well potentials, the term 'symmetric' is used with two different meanings and this may lead to some confusion. A double-well potential, in which both minima have the same value for the energy, is generally called a 'symmetric double-well potential'. On the other hand, in a 'symmetric hydrogen bond', the proton is situated in the middle between its two neighbours. Such a bond is represented by a single-minimum potential. Throughout this text the term 'symmetric hydrogen bond' is used in connection with a single-minimum potential, while 'symmetric' and 'non-symmetric' double-well potentials describe 'non-symmetric' hydrogen bonds.

[15] Gröne A and Kapphan S 1995 *J. Phys.: Condens. Matter* **7** 6393

[16] Nelmes R J, Loveday J S, Wilson R M, Besson J M, Pruzan Ph, Klotz S, Hamel G and Hull S 1993 *Phys. Rev. Lett.* **71** 1192

[17] Schäferjohann V 1990 *Thesis* Universität GH Paderborn

[18] Hydrogen bonds have been classified in reference [11], according to the bond length: $R > 270$ pm ('weak'), 260 pm $< R <$ 270 pm ('intermediate'), $R < 260$ pm ('strong'). This nomenclature is occasionally adopted here, because it finds physical support in the present model.

[19] Negative mode-Grüneisen parameters are not only typical of O–H$\cdots$O hydrogen bonds, but can also be found in other substances, e.g., the hydrogen halides (see references [20, 21]). For the interpretation, double-well potentials are also used in these cases [22].

[20] Johannsen P G, Helle W and Holzapfel W B 1984 *J. Physique Coll.* C8 199

[21] Johannsen P G, Helle W and Holzapfel W B 1990 *High Pressure Science and Technology* ed W B Holzapfel and P G Johannsen (London: Gordon & Breach) p 227

[22] Jansen R W, Bertoncini R, Pinnick D A, Katz A I, Hanson R C, Sankey O F and O'Keeffe M 1987 *Phys. Rev.* B **35** 9830

[23] Lee C, Vanderbilt D, Laason K, Car R and Parrinello M 1993 *Phys. Rev.* B **47** 4863

[24] Aoki K, Yamawaki H and Sakashita M 1996 *Phys. Rev. Lett.* **76** 784

[25] Hirsch K R and Holzapfel W B 1986 *J. Chem. Phys.* **84** 2771

[26] Aoki K, Yamawaki H, Sakashita M and Fujihisa H 1996 *Phys. Rev.* B **54** 15 673

[27] Horsewill T, Johnson M and Trommsdorff H P 1997 *Europhys. News* **28** 140 and references therein

[28] Benderskii V A, Makarov D E and Wight C A 1994 *Chemical Dynamics at Low Temperatures (Advances in Chemical Physics 88)* ed I Prigogine and S A Rice (New York: John Wiley)
[29] Smith D F and Overend J 1972 *Spectrochim. Acta* A **28** 471
[30] For asymmetric bonds, in which the proton is more closely connected to one of its neighbours, the use of these reduced masses is justified, but for the symmetric case, reduced masses, which take into account both neighbours, or even the bare proton and deuteron masses, may be more appropriate. However, this makes only a minor contribution and for the sake of uniformity the reduced masses, given in the text, have been used in all of the calculations.
[31] Klug D D, Mishima O and Whalley E 1987 *J. Chem. Phys.* **86** 5323
[32] Phillips W A 1981 *Amorphous Solids, Low-Temperature Properties* ed W A Phillips (Berlin: Springer) p 1
[33] Pruzan Ph 1994 *J. Mol. Struct.* **322** 279
[34] Hemley R J, Jephcoat A P, Mao H K, Zha C S, Finger L W and Cox D E 1987 *Nature* **330** 737
[35] Klug D D and Whalley J 1984 *J. Chem. Phys.* **81** 1220
[36] Schäferjohann V, Johannsen P G and Kapphan S 1998 to be published
[37] Goncharov A F, Struzhkin V V, Somayazulu M S, Hemley R J and Mao H K 1996 *Science* **273** 218
[38] Struzhkin V V, Goncharov A F, Hemley R J and Mao H K 1997 *Phys. Rev. Lett.* **78** 4446
[39] Mao H K and Hemley R J 1991 *Nature* **351** 721
[40] Hanfland M and Syassen K 1985 *J. Appl. Phys.* **57** 2752
[41] Lowndes R P and Rastogi A 1976 *Phys. Rev.* B **14** 3598
[42] Köhler U, Johannsen P G and Holzapfel W B 1997 *J. Phys.: Condens. Matter* **9** 5581
[43] Chen N H, Sterer E and Silvera I F 1996 *Phys. Rev. Lett.* **76** 1663
[44] Johannsen P G 1989 *Simple Molecular Systems at Very High Density* ed A Polian, P Loubeyre and N Boccara (New York: Plenum) p 277
[45] Schnakenberg J 1995 *Algorithmen in der Quantentheorie und Statistischen Physik* (Ulmen: Zimmermann-Neufang)
[46] An intrinsic linewidth of $\sigma_0 = 30$ cm^{-1} has been assumed (figure 13).
[47] Schutte C 1976 *The Quantum Mechanics and Group Theory of Vibrating and Rotating Molecules (The Theory of Molecular Spectroscopy 1)* (Amsterdam: North-Holland)